ADVANCED MATERIALS

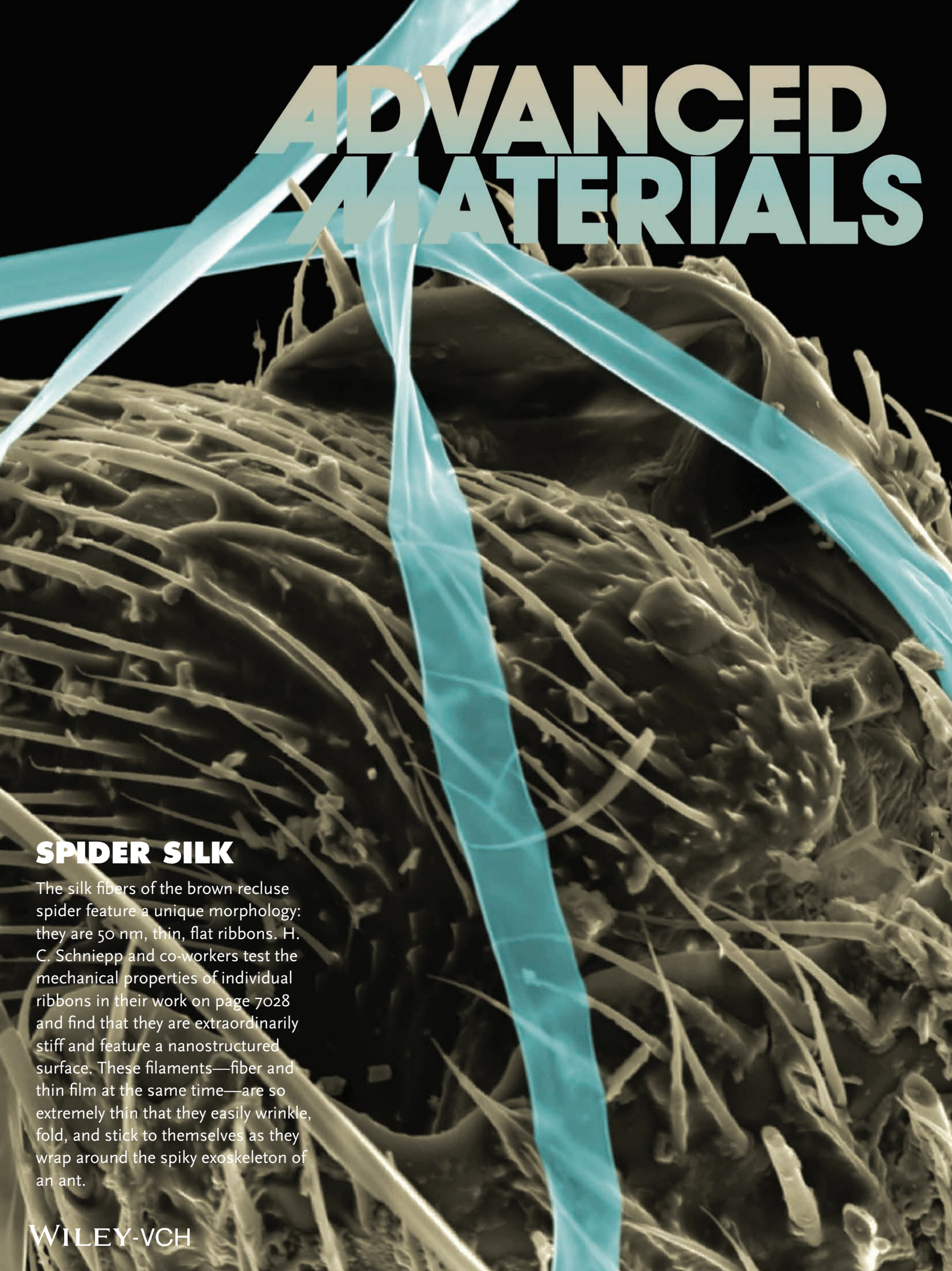

SPIDER SILK

The silk fibers of the brown recluse spider feature a unique morphology: they are 50 nm, thin, flat ribbons. H. C. Schniepp and co-workers test the mechanical properties of individual ribbons in their work on page 7028 and find that they are extraordinarily stiff and feature a nanostructured surface. These filaments—fiber and thin film at the same time—are so extremely thin that they easily wrinkle, fold, and stick to themselves as they wrap around the spiky exoskeleton of an ant.

WILEY-VCH

ADVANCED MATERIALS
www.advmat.de

www.MaterialsViews.com

Brown Recluse Spider's Nanometer Scale Ribbons of Stiff Extensible Silk

Hannes C. Schniepp, Sean R. Koebley, and Fritz Vollrath*

With oil reserves dwindling, the search for sustainable synthetic polymers 'fit for' the 21st century is accelerating.[1] With that in mind, biological polymer fibers like the dragline threads of the golden orb-spider are gaining increasing importance as model systems.[2–4] These naturally spun fibers are the result of co-evolved dope–extrusion systems, and the resulting filaments tend to be tough, skin–core composites of varying complexity.[5–7] With typically more than one protein in the mix, and diameters on the micrometer scale,[8] force–extension curves reveal complex viscoelastic behavior with a stiff initial modulus followed by varying degrees of work hardening,[2,9] depending on the molecular and supramolecular structures.[10–12] Moreover, the rate of spinning affects the bulk properties of the material, as does the level of hydration.[13–15]

In parallel to fundamental research into the properties of natural fibers, a large body of more product-oriented research is conducted on fibers spun and films cast from reconstituted silk solutions.[16] Because of the amounts of material required, such fibers and films typically are obtained not from spider silks but from mulberry silkworm threads that have been dissolved, dialyzed, and then subjected to other bespoke treatments.[17] Such reconstituted silk fibers and films tend to be several micrometers thick, and, especially, the films have led to a surprising variety of devices with great potential ranging from dedicated tissue scaffolds to implantable bioelectronic devices.[4,18,19] The main drawback of reconstituted silk-based fibers are their material properties, which compare unfavorably with those of native silk threads unless they receive considerable un-biological post-draw treatments.[20,21] Importantly, until now there were no examples of native silk films naturally extruded through an evolved production system, so there was no possibility of estimating the inherent mechanical properties possible for such films.

In this work, we examined the film ribbons spun by the brown recluse spider *Loxosceles laeta*, which are up to 10 μm wide and have thicknesses of a few tens of nanometers.[22,23] This material allowed us to investigate two problems with one sample; we can: a) study the mechanical properties of naturally spun fiber-silk without any confounding skin–core properties, and b) measure the intrinsic characteristics of a well-spun silk film. The results are truly surprising. Interesting and potentially new questions are raised not only by the behavior of the ribbons, but also by some of the associated novel nanostructures discovered during this study.

Information on the structure and properties of *Loxosceles* ribbon silk in the literature is scarce, as only two prior reports present structural evidence of these interesting filaments and their natural production systems.[22,23] We are the first to report direct extraction of silk fibers from these animals, which allows us to manipulate ribbon parameters via controlling the spinning conditions. Moreover, this controlled extraction of the ribbons from the animals enables us to perform sophisticated experiments with these materials, such as contacting the fiber with other materials or devices in a controlled manner. **Figure 1**a features a scanning electron microscropy image revealing several of the outstanding properties of the fiber: it is a thin, flat ribbon of uniform width. Figure 1b depicts several strands of the ribbon at higher magnification, revealing that it is only a few 10 nm thick. Figure 1c illustrates that these ribbons can easily bend and wrinkle, since they are extremely thin. Especially for stretched ribbons, we observed a considerable degree of wrinkling, suggesting that they undergo strain-induced crimping.

For quantitative, high-resolution structural characterization of the fibers we employed atomic force microscopy (AFM). **Figure 2**a depicts a 3D-rendered AFM topography image of a fiber, featuring the edge of a ribbon (golden-colored structure on the right hand side) placed on a glass substrate (dark brown, left hand side). The thickness and width of the ribbons was determined on the basis of AFM topography sections running perpendicularly across entire fibers (Figure 2b). The *Loxosceles* ribbons we studied were 40–80 nm thick with widths in the range of 6–9 μm. Dimensional fluctuations between fibers from a particular animal taken at different times are significantly less than the fluctuations between fibers from different animals. Narrower fibers are consistently thinner than wider fibers; the cross-sectional aspect ratios of all fibers measured are in the range 1:100–1:150 (see Supporting Information for details).

The ribbon-like morphology of the *Loxosceles* silk fiber featuring an extreme aspect ratio makes this material unique in several respects. While also produced by major ampullate (MA) glands, albeit through a flattened spinneret,[23] this morphology represents a stark contrast to the silks of other spider species. Comparably sized orb-weaving araneids produce MA silks of cylindrical symmetry with diameters on the order of one to several micrometers,[8] which feature complex structures, typically with semihierarchical skin–core morphologies

Prof. H. C. Schniepp, S. R. Koebley
Department of Applied Science
The College of William & Mary, PO Box 8795
Williamsburg, VA, 23187, USA
E-mail: schniepp@wm.edu
Prof. F. Vollrath
Department of Zoology
University of Oxford
South Parks Rd, OX1 3PS, UK

DOI: 10.1002/adma.201302740

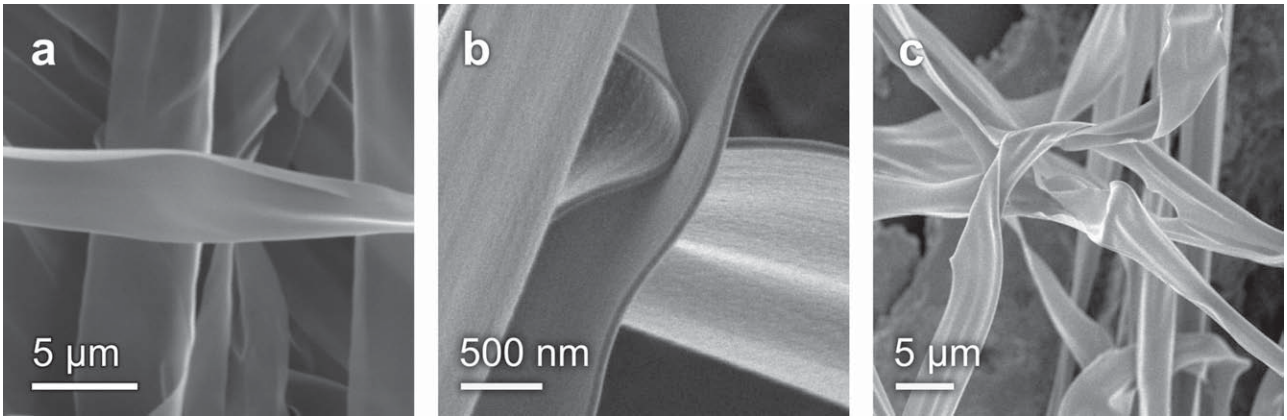

Figure 1. The silk of the *Loxosceles* spider makes thin ribbons with an aspect ratio of 100:1 and above. a) Scanning electron microscopy (SEM) image featuring several ribbons. b) Side view showing the thinness of the ribbon. c) Due to their thinness, the fibers bend and wrinkle easily.

containing inclusions, nanofibrils, and layers of coatings.[5,6] In contrast, *Loxosceles* silk ribbons with thicknesses of several tens of nanometers can accommodate only a few layers of protein molecules from top to bottom; this implies a much simpler silk structure. Unlike artificial silk films, the loxo-ribbons are extrusion-spun from raw silk. Due the thinness of the ribbons, all of the *Loxosceles* silk dope is in close proximity to the walls of the spinneret during the extrusion process, where strong shear differentials induce structural changes in the protein.[24,25] For regular, cylindrical silk, this happens only in the periphery of the fiber; it is thus likely that the silk in the loxo-ribbons essentially corresponds to the peripheral ("shell") component of regular silk. *Loxosceles* silk ribbons are thus an ideal model system to investigate the fundamentals of "silk", especially since their flatness facilitates a wide range of experimental procedures that are unavailable or difficult to apply to a cylinder. Importantly, the flat loxo-ribbons are exceptionally suited for investigation via scanning probe techniques to reveal further structural details. The tapping-mode AFM data shown in Figure 2a and 2c reveals a fibrillar surface texture of the fibers with an average center-to-center distance of 11 ± 2 nm between individual fibrils. This fibrillar structure is confirmed by our SEM data (Figure 2d and 2e) and is in agreement with previous transmission electron microscopy (TEM) evidence.[23] A similar fibrillar morphology

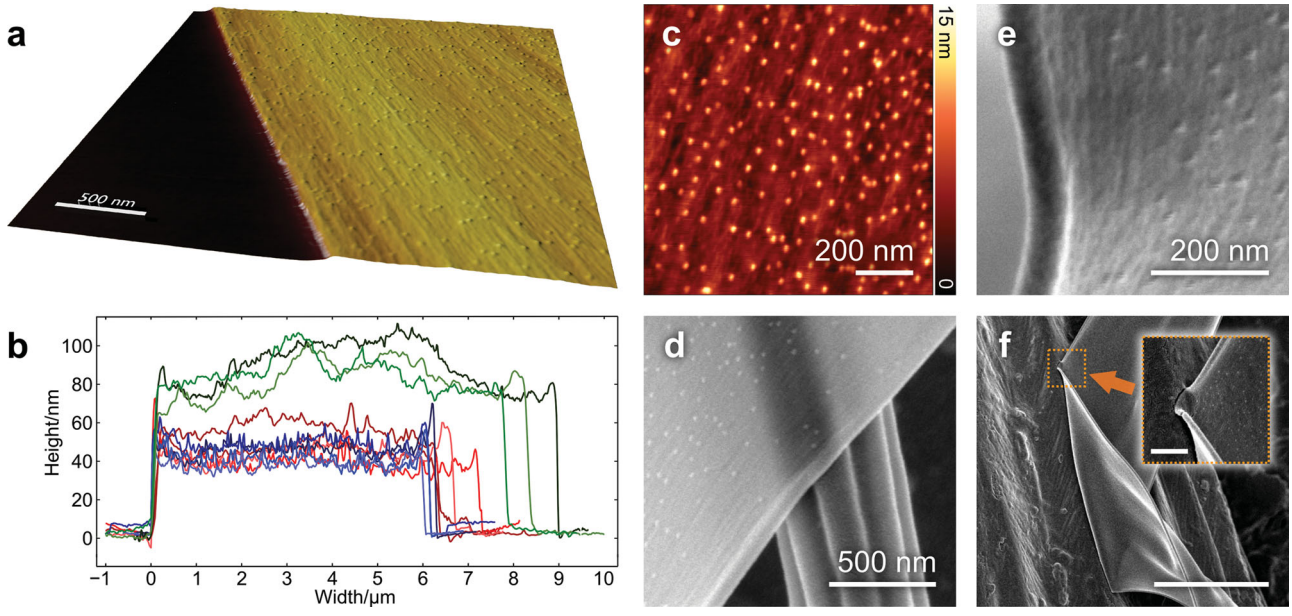

Figure 2. a) Tapping-mode AFM topography image featuring a ribbon (golden) placed on a glass substrate (dark brown). The scale bar applies for lateral and vertical directions. b) AFM topography sections across different fibers. Each of the color families red, blue, and green corresponds to a separate individual. c–e) "Nanopapillae" featured in detail by AFM topography (c) and scanning electron microscopy (SEM) (d,e). f) The papillae may contribute to the good adhesive properties revealed by the SEM image showing a *Loxosceles* ribbon adhered to the elytron of an *Alaus oculatus* beetle (scale bar: 5 µm). Inset: higher magnification of the area highlighted in the orange dotted square (scale bar: 500 nm).

has been discovered on the surface of silks with cylindrical morphology,[5,11,26] supporting our hypothesis that the *Loxosceles* ribbons are similar to the outer layers found in other silks.

In addition to the fibrillar surface texture, our AFM imagery also reveals surface structures that were not previously reported for any silk: point-like surface features, "nanopapillae", that ubiquitously populate the ribbon surfaces (Figure 2a and Figure 2c). They protrude at a height of 7.0 ± 1.2 nm (n = 25), which is substantial compared to the 40–80 nm total thickness of the fiber. Furthermore, with an apparent diameter of about 15 nm, it is probable that the papillae have an aspect ratio around 1, since AFM typically underestimates the height and overestimates the width of nanometer-scale objects.[27] The corroboration of these structures via SEM imaging (Figure 2d,e), a technique which, unlike AFM, has been extensively applied to other silks, asserts that the nanopapillae are likely unique to the *Loxosceles* genus.

We suspect that these nanopapillae give rise to a particular property of the material. One preliminary hypothesis offers that the nanopapillae alter the adhesive properties of the fiber. Investigations of synthetic thin films provide potentially relevant evidence suggesting that surface features of similar morphology (but orders of magnitude larger in size) can significantly enhance adhesion.[28–30] Indeed, our evidence indicates that the *Loxosceles* ribbons exhibit strong adhesion. Figure 2f shows an SEM image of a ribbon attached to the elytron of an *Alaus oculatus* beetle. Clearly visible in the inset, the adhesion in the contact area is strong enough to deform the adhered ribbon significantly. We conjecture that the thinness of the ribbon and its resulting capability of deforming easily promote enhanced adhesion: due to its flexibility, the ribbon can conform to the surface topography of objects it contacts. Consequently, it can establish adhesive contact over a larger area in comparison to thicker, less flexible materials. Hence, the *Loxosceles* ribbons represent a unique model system to study a molecularly thin, free-standing, mechanically strong polymer film and the resulting adhesive properties.

Measuring the tensile performance of the *Loxosceles* ribbons is challenging, since they feature cross-sections on the order of 4 × 10^{-13} m^2 = 0.4 $(\mu m)^2$, about 20–30 times less than other silk fibers. In order to achieve the necessary force resolution, we thus devised an AFM-based method capable of performing tensile characterization of individual *Loxosceles* ribbons. Similar techniques have successfully been employed to determine the mechanical properties of suspended biopolymer fibers.[31,32] *Loxosceles* ribbons were placed on glass substrates featuring a trench with a width of several 100 µm and a depth of about 200 µm. The ribbons were manually positioned perpendicularly across the trench, such that a portion of the fiber was freely suspended (**Figure 3**a). Care was taken to avoid straining the ribbons. A blunted AFM probe was then landed on the silk ribbon in the middle of the suspended portion, as shown in Figure 3b. Lowering the AFM probe from this position stretches the silk ribbon, thus increasing the tensile stress σ in the fiber. This tensile stress leads to a vertical force F_{vert} acting toward restoration of the relaxed state of the fiber (see Figure 3b). By acquiring an AFM force curve, F_{vert} is measured as a function of the indentation depth h. The tensile force F_T in the fiber can be calculated from $F_{vert}(h)$, and the strain ε in the fiber can be calculated from h. Thus, we can deduce the stress–strain behavior $\sigma(\varepsilon)$ of *Loxosceles* silk from the measured $F_{vert}(h)$ curves.

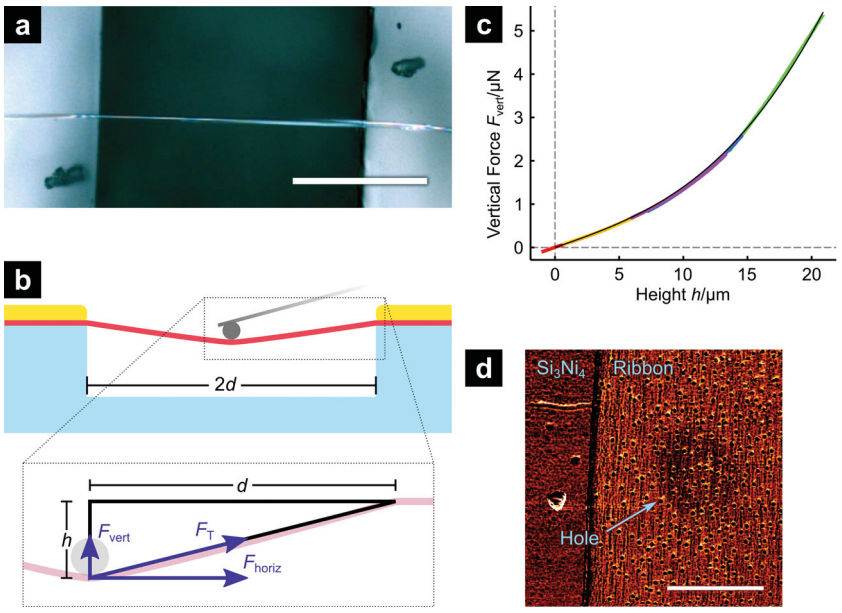

Figure 3. a) Top view of the mechanical testing setup (optical micrograph). Scale bar: 200 µm. b) Schematic of the setup: a *Loxosceles* fiber (rose) was suspended over a gap in a glass substrate (light blue) and secured with cyanoacrylate glue (amber). A blunted AFM probe (grey) strained the silk via vertical deflection, while simultaneously measuring the vertical component F_{vert} of the fiber tensile force F_T as a function of the probe indentation height h. c) Obtained force curves (various colors) and the fitted model (black). d) AFM tapping-mode phase image of a silk ribbon suspended over a 1 µm-diameter hole in a silicon nitride substrate. The ribbon covers the hole and can sustain forces exerted by the AFM probe. Phase imaging reveals the position of the hole since the ribbon deflects in the suspended area (scale bar: 1 µm).

A set of force curves $F_{vert}(h)$ measured for the suspended silk fiber is shown in Figure 3c. $F_{vert}(h)$ is strongly non-linear, for two reasons related to the geometry of the setup. Firstly, the relation between the vertical fiber deflection h and the induced strain $\varepsilon = \varepsilon(h)$ is non-linear: $\varepsilon(h) = \sqrt{1 + \frac{h^2}{d^2} \cdot (1 + \varepsilon_{pre})} - 1$, where ε_{pre} and d are the fiber pre-strain and the half width of the gap, respectively. The corresponding fiber tensile force is $F_T(h) = \sigma[\varepsilon(h)] \times A$, where $\sigma[\varepsilon]$ is the stress–strain relationship of the material and A is the cross-sectional area of the fiber. The second reason for the observed non-linearity is that $F_{vert}(h)$ essentially represents the vertical projection of F_T: $F_{vert}(h) = 2 \cdot \sigma[\varepsilon(h)] A \cdot h / \sqrt{h^2 + d^2}$. The AFM probe is positioned at the midpoint of the suspended ribbon, dividing it into two halves. We independently consider contributions of both halves to F_{vert}, giving rise to the factor of 2. The tensile forces F_T in the fiber do not give rise to a net horizontal force on the AFM probe, since horizontal components F_{horiz} of F_T contributed by the two halves cancel out.

The maximal strains in our experiments were in the range 0.68–0.98%, which led us to assume a linear stress–strain relationship $\sigma[\varepsilon] = E \cdot \varepsilon$, where E is Young's modulus. The pre-strain ε_{pre} can be eliminated for this particular geometry by considering the case $h/d << 1$, for which $F_{vert}(h) \approx 2AE \cdot \varepsilon_{pre} h/d$, and thus ε_{pre} can be expressed in terms of the initial slope of the measured $F_{vert}(h)$ curve. Since experimental determination of d and A is straightforward, the modulus E remains the only unknown, which we determined by carrying out non-linear least squares fits to the measured $F_{vert}(h)$ curves. The agreement between the experimental data and the obtained fits is excellent (see Figure 3c), which justifies the assumption of a linear stress-vs-strain relation. Averaged over several experiments carried out on ribbons from different specimens, we determined the Young's modulus of *Loxosceles* silk to be $E = 21 \pm 6$ GPa, with corresponding pre-strains in the range 0.16–0.35%. We found that repeated acquisition of force curves led to virtually identical results, which demonstrates that the *Loxosceles* ribbons are fully elastic in the studied strain regime (for details see the Supporting Information). This fully elastic behavior and repeatability allowed us to acquire data for indentation ranges >30 μm, significantly exceeding the vertical range of our piezo scanner (10 μm). Several 10 μm-deep portions of the force curve – each represented by a different color in Figure 3c – were therefore acquired, offset by mechanical translations between them. Due to its high force sensitivity and good control over small translations, AFM is an excellent tool for characterizing the mechanical properties of the *Loxosceles* ribbons in the realm of small strains.

In addition to the modulus, we also determined the maximum extensibility of the material to be $27.4 \pm 2.7\%$ ($n = 4$) by straining individual strands to fracture. A modulus of 21 ± 6 GPa and the maximum extensibility of 25–30% suggest that *Loxosceles* silk is extremely strong and tough; these values are among the highest for any silk, similar to those found for orb-weaving silk.[33] Hence, the loxo-ribbons feature the trademark of silk's extraordinary mechanical properties, the combination of high stiffness with large extensibility. This is remarkable because it would not be surprising to see substantial differences in the fracture mechanics between these 40–80 nm-thin ribbons with a 100:1 aspect ratio on the one hand, and all other silk fibers featuring cylindrical geometry and a skin–core structure, on the other. A possible explanation for these high stiffness values in the loxo-ribbons is that the regular silks with their core–shell structure may contain a larger fraction of low-modulus components, whereas *Loxosceles* silk may feature a purer mixture of high-modulus material. In particular, the loxo-ribbons are far superior to currently available, artificial silk thin films in terms of their mechanical properties. The strongest ultrathin films of reconstituted silkworm silk yield a modulus of 3–5 GPa and maximum extensibility of only 0.5–3%.[21,34] These data suggest that the strength of the loxo-ribbons is 1 to 2 orders of magnitude superior to their artificial counterparts. Engineered thin silk films, modeled on the loxo-ribbons, and with similarly outstanding mechanical properties would have many interesting applications, such as tissue scaffolds with tunable mechanical properties and electronic brain implants.[4,18,19,35] To feature the film-like properties of the *Loxosceles* ribbons, we suspended ribbons on a silicon nitride substrate with 1 μm-diameter holes (Figure 3d). The film covers the hole and withstands forces exerted through repeated AFM scanning in contact and tapping imaging modes.

The thinness of the loxo-ribbons also has significant implications transcending the investigation of silk. Several recent reports have shown that polymers exhibit thermal or mechanical properties substantially different from bulk behavior when they are in the vicinity of a surface or an interface.[36] In particular, this applies to polymer thin films with thicknesses of several 10 nm. The loxo-ribbons are an interesting system to test for this behavior in a biopolymer, since they are thin to the point that the majority of the protein material is within nanometers of the surface.

In conclusion, the naturally spun ribbon of *Loxosceles* silk is likely to inspire the next generation of artificial silk films. It demonstrates that if extrusion-spun by a highly developed production system, nanometer-thin films can reach the performance properties of the best silk fibers known. Importantly, featuring disparate dimensions and a peculiar dotted surface, the loxo-ribbons mark an exciting departure from the norms of major ampullate silk. Nevertheless, in their fibrillar structure and impressive mechanical properties, they clearly share much in common with silk archetypes, and may therefore serve as a novel system from which general conclusions of universal silk structure may be drawn. A unique natural hybrid of fiber and film, of orthodoxy and novelty, *Loxosceles* silk promises an exciting new avenue for silk research.

Experimental Section

Spider Care and Silk Collection: Specimens of *Loxosceles laeta* were housed separately in capsules with strips of cotton cloth and were fed a weekly diet of crickets. Silk strands were obtained by collection or forcible reeling. Collection involved simply passing the substrate through a portion of the cobweb architecture or tweezing out free strands; forcible reeling was conducted as previously described[37] on a custom reel at 0.5 cm/s.

Scanning Electron Microscopy: Samples for SEM were made by collecting or reeling silk and placing it onto a *Drosophila melanogaster* wing and an *Alaus oculatus* elytron. These samples were then sputter-coated for 7 min with an Au–Pd target and imaged at 3 kV with a FE-SEM (Hitachi S4700).

Atomic Force Microscopy: An Ntegra Prima AFM (NT-MDT) configured with a Universal scanning head and a 100 μm × 100 μm × 10 μm closed-loop piezo scanner was employed for contact- and tapping-mode imaging, and to acquire the force curves. SiNi-type probes (BudgetSensors) with a tip radius <15 nm and a spring constant of 0.27 N/m were utilized in contact-mode. Type ACTA Si probes (AppNano) with ≈6 nm tip radius and a nominal spring constant of 40 N/m were used in tapping-mode. The AFM was operated in air with controlled 30–50% levels of relative humidity.

Setup for Modulus Measurement: For each modulus measurement a silk fiber was extracted from a spider and placed on top of a glass substrate featuring a trench (for details see Supporting Information). To prevent slippage, the silk fibers were glued to the substrate using cyanoacrylate glue (Duro). Surface tension pinned a glue droplet at both edges of the trench, preventing it from spreading onto the suspended part of the fiber. Excess glue was removed immediately by placing the sample on a spin-coater (Laurell WS-400Bz-6NPP). The suspended part of the ribbon was positioned on the rotation axis of the spin-coater so that the centrifugal spinning forces accelerated the glue droplet away from the suspended ribbon. The length of each suspended silk ribbon was measured via optical microscopy. The cross-sectional area of each ribbon was determined from AFM topography scans taken in the vicinity of the suspended region.

AFM Probes Used for Modulus Measurement: Type ACTA AFM probes (AppNano, nominal spring constant k = 40 N/m, cantilever length L = 140 µm) were customized for stress–strain analysis of suspended ribbons. First, the spring constant of each cantilever was calibrated using Sader's method;[38] the measured spring constants were in the range k = 19–23 N/m. We followed the method of Heim and coworkers to correct all the measured forces for the 15° cantilever tilt in our instrument.[39,40]

In order to avoid puncturing the silk ribbons with these very sharp and stiff probes, we blunted the tips after completing the spring constant calibration by dipping them into liquid epoxy resin (ACE quick setting epoxy) under an iX-71 inverted optical microscope (Olympus). This procedure formed an epoxy droplet with a diameter of 30–40 µm at the end of the cantilever, which was subsequently cured. The cured tips were inspected via optical microscopy before use. Using the built-in optical microscope of the AFM, these probes were then positioned midway on the suspended silk ribbon. Based on the effective contact point of each ribbon on the cantilever, an additional correction to the spring constant was applied (for details see the Supporting Information).

Force Spectroscopy: The force curves had a range of 7.5 µm and were acquired at a velocity of 1.5 µm/sec, operating the piezo scanner in closed-loop mode laterally and vertically. For fiber indentations exceeding the 10 µm vertical piezo range we also utilized the vertical coarse positioning system based on a motorized screw. This was done in several stages, in which the screw was used first to carry out a larger translation of several micrometers, followed by the acquisition of additional force curves. The force curves from each of these stages (each depicted using a different color in Figure 3c) were then combined to one master curve reflecting a total indentation range >30 µm (for details see Supporting Information).

Analysis of Force Data: The deflection sensitivity of the AFM was calibrated for each experiment by acquiring force curves directly on the glass substrate and determining the slope of the constant compliant regime.[41] Force–displacement curves were converted to force–distance curves.[41] Due to the design of this experiment, the maximal cantilever deflection was as small as about 200 nm, even for indentation depths exceeding 30 µm; therefore, this conversion yielded unusually small corrections.

Maximum Extensibility: The maximum extensibility of the ribbons was determined by placing them on a custom-made extensibility rig in a relaxed state and stretching the fiber continuously using a screw. This procedure was observed using an optical microscope and continued until failure of the fiber, similar as previously described.[42] All the lengths were measured using digital calipers (Carrera Precision).

Supporting Information

Supporting Information is available from the Wiley Online Library or from the author.

Acknowledgements

The authors thank Rick Vetter for providing Loxosceles specimens, Matthew Wawersik for a *Drosophila* sample, David Porter for providing feedback on the manuscript, Michael Funk and NASA Langley's Advanced Materials & Processing Branch for their electron microscopy support. F.V. thanks the AFOSR (FA9550–12–1–0294 06) and ERC (SP2-GA-2008–233409) for generous funding. H.C.S. thanks the Jeffress Memorial Trust (J-1012) for financial support.

Received: June 17, 2013
Revised: August 12, 2013
Published online: October 8, 2013

[1] R. A. Kerr, *Science* **2011**, *331*, 1510.
[2] F. Vollrath, D. Porter, *Soft Matter* **2006**, *2*, 377.
[3] C. Viney, *Supramol. Sci.* **1997**, *4*, 75.
[4] F. Omenetto, D. Kaplan, *Science* **2010**, *329*, 528.
[5] F. Vollrath, T. Holtet, H. C. Thogersen, S. Frische, *Proc. Biol. Sci.* **1996**, *263*, 147.
[6] A. Sponner, W. Vater, S. Monajembashi, E. Unger, F. Grosse, K. Weisshart, *PloS One* **2007**, *2*, e998.
[7] B. Swanson, T. Blackledge, J. Beltrán, C. Hayashi, *Appl. Phys. A* **2006**, *82*, 213.
[8] M. Heim, L. Römer, T. Scheibel, *Chem. Soc. Rev.* **2010**, *39*, 156.
[9] M. Denny, *J. Exp. Biol.* **1976**, *65*, 483.
[10] F. Vollrath, D. Porter, *Appl. Phys. A* **2006**, *82*, 205.
[11] N. Du, Z. Yang, X. Y. Liu, Y. Li, H. Y. Xu, *Adv. Mater.* **2011**, *21*, 772.
[12] F. G. Omenetto, D. L. Kaplan, *Nat. Mater.* **2012**, *11*, 273.
[13] R. Work, *Text. Res. J.* **1977**, *47*, 650.
[14] F. Vollrath, *Naturwissenschaften* **1991**, *78*, 557.
[15] K. J. Koski, P. Akhenblit, K. McKiernan, J. L. Yarger, *Nat. Mater.* **2013**, *12*, 1.
[16] H. Tao, D. L. Kaplan, F. G. Omenetto, *Adv. Mater.* **2012**, *24*, 2824.
[17] H.-J. Jin, D. L. Kaplan, *Nature* **2003**, *424*, 1057.
[18] J. G. Hardy, L. M. Römer, T. Scheibel, *Polymer* **2008**, *49*, 4309.
[19] D.-H. Kim, J. Viventi, J. J. Amsden, J. Xiao, L. Vigeland, Y.-S. Kim, J. A. Blanco, B. Panilaitis, E. S. Frechette, D. Contreras, D. L. Kaplan, F. G. Omenetto, Y. Huang, K.-C. Hwang, M. R. Zakin, B. Litt, J. A. Rogers, *Nat. Mater.* **2010**, *9*, 511.
[20] F. Vollrath, D. Porter, C. Holland, *Soft Matter* **2011**, *7*, 9595.
[21] C. Jiang, X. Wang, R. Gunawidjaja, Y.-H. Lin, M. K. Gupta, D. L. Kaplan, R. R. Naik, V. V. Tsukruk, *Adv. Funct. Mater.* **2007**, *17*, 2229.
[22] J. A. Coddington, H. D. Chanzy, C. L. Jackson, G. Raty, K. H. Gardner, *Biomacromolecules* **2001**, *3*, 5.
[23] D. P. Knight, F. Vollrath, *Philos. Trans. R. Soc. London, Ser. B* **2002**, *357*, 219.
[24] A. Sponner, E. Unger, F. Grosse, K. Weisshart, *Nat. Mater.* **2005**, *4*, 772.
[25] I. Greving, M. Cai, F. Vollrath, H. C. Schniepp, *Biomacromolecules* **2012**, *13*, 676–682.
[26] S. F. Li, A. J. McGhie, S. L. Tang, *Biophys. J.* **1994**, *66*, 1209.
[27] S. Santos, V. Barcons, H. K. Christenson, J. Font, N. H. Thomson, *PloS One* **2011**, *6*, e23821.
[28] A. J. Crosby, M. Hageman, A. Duncan, *Langmuir* **2005**, *21*, 11738.
[29] A. Mahdavi, L. Ferreira, C. Sundback, J. W. Nichol, E. P. Chan, D. J. D. Carter, C. J. Bettinger, S. Patanavanich, L. Chignozha, E. Ben-Joseph, A. Galakatos, H. Pryor, I. Pomerantseva, P. T. Masiakos, W. Faquin, A. Zumbuehl, S. Hong, J. Borenstein, J. Vacanti, R. Langer, J. M. Karp, *Proc. Natl. Acad. Sci. USA* **2008**, *105*, 2307.
[30] H. Shahsavan, B. Zhao, *Soft Matter* **2012**, *8*, 8281.
[31] G. Guhados, W. Wan, J. L. Hutter, *Langmuir* **2005**, *21*, 6642.
[32] J. F. Smith, T. P. J. Knowles, C. M. Dobson, C. E. Macphee, M. E. Welland, *Proc. Natl. Acad. Sci. USA* **2006**, *103*, 15806.
[33] I. Agnarsson, M. Kuntner, T. a Blackledge, *PloS One* **2010**, *5*, e11234.
[34] E. Kharlampieva, V. Kozlovskaya, B. Wallet, V. V. Shevchenko, R. R. Naik, R. Vaia, D. L. Kaplan, V. V Tsukruk, *ACS Nano* **2010**, *4*, 7053.
[35] L. W. Tien, F. Wu, M. D. Tang-Schomer, E. Yoon, F. G. Omenetto, D. L. Kaplan, *Adv. Funct. Mater.* **2013**, *23*, 3185.
[36] P. O'Connell, G. McKenna, *Science* **2005**, *307*, 1760.
[37] R. Work, P. Emerson, *J. Arachnology* **1982**, *10*, 1.
[38] J. E. Sader, J. W. M. Chon, P. Mulvaney, *Rev. Sci. Instrum.* **1999**, *70*, 3967.
[39] L.-O. Heim, M. Kappl, H.-J. Butt, *Langmuir* **2004**, *20*, 2760.
[40] J. L. Hutter, *Langmuir* **2005**, *21*, 2630.
[41] B. Cappella, G. Dietler, *Surf. Sci. Rep.* **1999**, *34*, 1.
[42] J. Pérez-Rigueiro, C. Viney, J. Llorca, M. Elices, *J. Appl. Poly. Sci.* **1998**, *70*, 2439.